International Journal of Fluid Machinery and Systems
Vol. 2, No. 4, October-December 2009

Original Paper

Large Eddy Simulation of the Dynamic Response of an Inducer to Flow Rate Fluctuations

Donghyuk Kang[1], Koichi Yonezawa[1], Tatsuya Ueda[1], Nobuhiro Yamanishi[2], Chisachi Kato[3], Yoshinobu Tsujimoto[1]

[1]Graduate School of Engineering Science, Osaka University
1-3 Machikaneyama, 560-8531, Toyonaka, Osaka, Japan
[2] Japan Aerospace Exploration Agency,
2-1-1, 305-8505, Sengen, Tsukuba, Japan
[3]Institute of Industrial Science, Tokyo University
4-6-1, Komaba, Meguro-ku, 153-8505, Tokyo, Japan

Abstract

A Large Eddy Simulation (LES) of the flow in an inducer is carried out under flow rate oscillations. The present study focuses on the dynamic response of the backflow and the unsteady pressure performance to the flow rate fluctuations under non-cavitation conditions. The amplitude of angular momentum fluctuation evaluated by LES is larger than that evaluated by RANS. However, the phase delay of backflow is nearly the same as RANS calculation. The pressure performance curve exhibits a closed curve caused by the inertia effect associated with the flow rate fluctuations. Compared with simplified one dimensional evaluation of the inertia component, the component obtained by LES is smaller. The negative slope of averaged performance curve becomes larger under unsteady conditions. From the conservations of angular momentum and energy, an expression useful for the evaluation of unsteady pressure rise was obtained. The examination of each term of this expression show that the apparent decrease of inertia effects is caused by the response delay of Euler's head and that the increase of negative slope is caused by the delay of inertial term associated with the delay of backflow response. These results are qualitatively confirmed by experiments.

Keywords: Inducer, Backflow Vortex, Dynamic Response to flow rate fluctuation, Large Eddy Simulation

1. Introduction

In turbo-pumps for rocket engines, an inducer is installed to prevent the head drop of the main pump impeller caused by cavitation. Inducers often have a swirling backflow in a wide range of flow rates because they are designed with a positive incidence angle even at the design point in order to attain high cavitation performance. Backflow from the inducer has a swirl velocity of about 20-30% of tip velocity and a backflow vortex structure is formed at the shear layer between swirling backflow and straight main flow. Experimental and computational studies of the backflow and backflow vortex of inducer have been reported [1-3].

Cavitation causes instabilities such as cavitation surge and rotating cavitation in the range where the head is not yet decreased [4]. In order to prevent the cavitation instabilities, leading edge sweep [5] and inlet casing enlargement [6] are often used. These methods cause larger amount of backflow. However, the relationship between the increase of backflow and suppression of the cavitation instabilities is not clear.

In the past research, Qiao et al. investigated the response of backflow to the flow rate fluctuation by using an unsteady CFD results based on RANS [2]. Although the computational results showed many reasonable agreements with experimental results, the excessive eddy viscosity caused by RANS did not allow to simulate the backflow vortices. In the present work, a Large Eddy Simulation (LES) is applied in order to investigate the dynamic response of inducer to flow rate oscillations under the occurrence of backflow vortices.

Received March 27 2009; Accepted for publication July 29 2009: Review conducted by Prof. Youn-Jea Kim. (Paper number O09019)
Corresponding author: Mr. Donghyuk Kang, kang@me.es.osaka-u.ac.jp

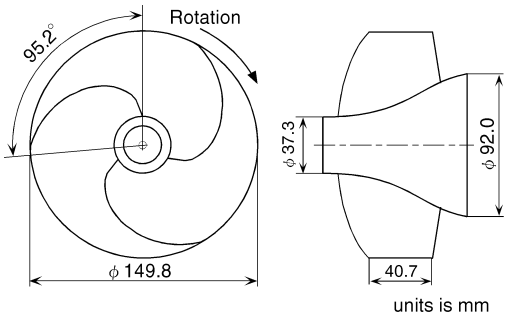

Fig. 1 Geometry of inducer

Table 1 Design parameter of inducer

Number of blades	3
Tip diameter (D_t) (mm)	149.8
Inlet tip blade angle, β_{1t}(deg)	7.5
Outlet tip blade angle, β_{2t}(deg)	9.0
Hub / Tip ratio at inlet	0.25
Hub / Tip ratio at outlet	0.51
Solidity at tip	1.91
Design flow coefficient, ϕ_d	0.078

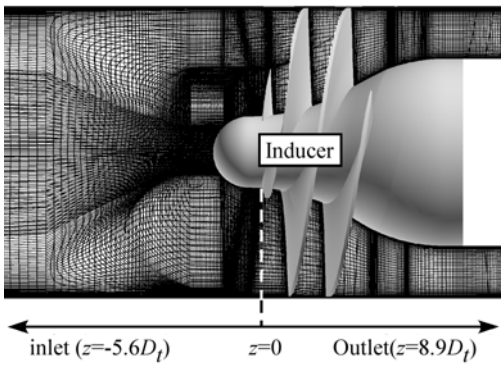

Fig. 2 Computational mesh around inducer

Table 2 Computational schemes of LES3C

Working Fluid	Water (Non-cavitation)
Pressure coupling	Fractional step method with low Mach number approximation (M=0.015)
FEM formulation	Crank Nicolson scheme and standard Galerkin method (2nd order accuracy in space and time)
SGS turbulence model	Standard Smagorinsky model (Cs=0.15)

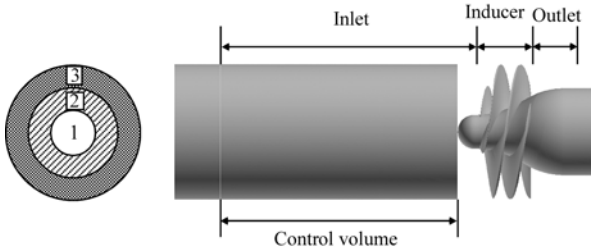

Fig. 3 Schematic of control volume upstream of inducer

2. Computational and Experimental Methods

Main dimensions of the inducer used in computations and experiments are shown in Fig.1 and Table 1. The inducer has three helical blades with the swept leading edge, with the tip diameter of 149.8mm and radial tip clearance of 0.5mm. The inlet and outlet blade angles are 7.5 and 9.0 degrees at the blade tip respectively, and the angle of sweep back is 95 degree. The distribution of blade angle $\beta(r)$ follows the helical condition, $r\times\tan\beta(r)=R_t\times\tan\beta_t$. The design flow coefficient is ϕ_d=0.078.

2.1 Computational Method

LES3C of FrontFlow/blue [7] is used for the simulation of the unsteady noncavitating flow of the inducer. The governing equation is based on the spatially-filtered continuity and Navier-Stokes equations for the flow of an incompressible fluid. The Crank Nicolson scheme and standard Galerkin method is used to discretize the governing equations, with the unstructured hexahedral meshes. The computational schemes in the present study are shown in Table 2. The single phase liquid is assumed as the working fluid. The pressure is calculated by the Fractional step method with low Mach number approximation (M=0.015) and the second order schemes in space and time are used. The effect of eddy viscousity is modeled with the standard Smagorinsky model with C_s=0.15, which is a standard value for flows with large separation, and incorporated with the Van-Driest wall-damping function representing the near-wall effect. The filter size is computed as the cubic-root of the volume of each finite element.

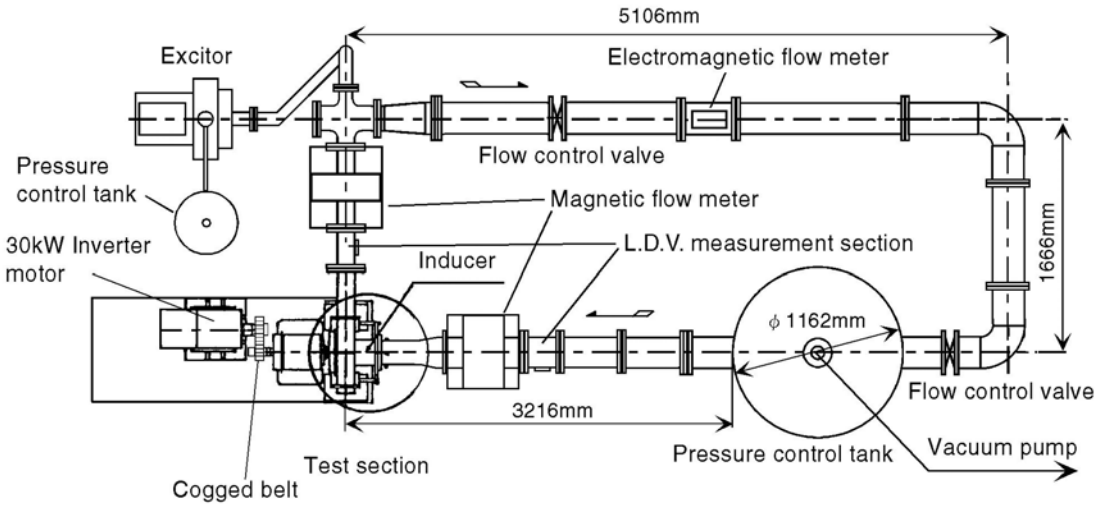

Fig. 4 Test facility

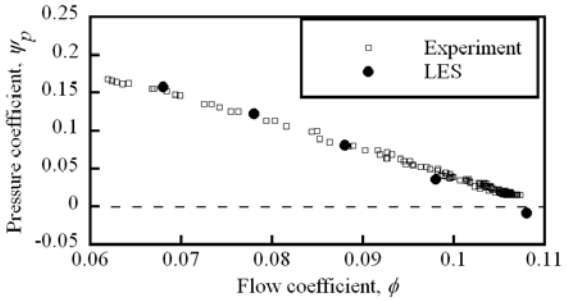

Fig. 5 Static pressure performance curve

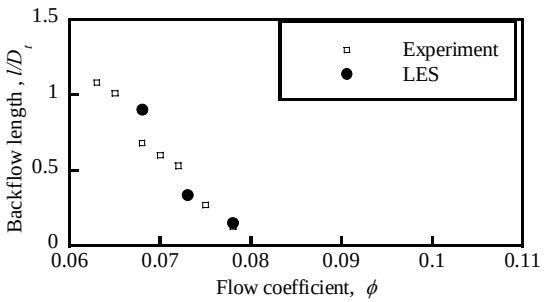

Fig. 6 Backflow length versus flow coefficient

Figure 2 shows the computational mesh around the inducer including all the blades. The number of computational cells is about 5,500,000. The lengths of inlet and outlet pipes are about 5.6 and 8.9 times the inducer diameter. The rotating speed is fixed at 4000 rpm. The axial velocity at inlet and the pressure at outlet are imposed as boundary conditions. Non-slip boundary condition is imposed on the walls. The axial coordinate z is set in the direction of flow with the origin (z/D_t=0) at the leading edge of blades at hub. In order to investigate the delay of acceleration term, the schematic of radially divided control volumes upstream of inducer ($1.9< z/D_t <0$) are shown in Fig.3.

2.2 Experimental Method

Figure 4 shows the schematic of the test facility used for experiments. The working fluid is water at room temperature. The mean flow rate is adjusted by the flow control valve. The excitor to generate flow rate oscillations is located at downstream. The inlet flow oscillation is measured by the magnetic flow meter installed at upstream (z/D_t=-6.6). The inlet and outlet pressure oscillations are measured by flush mounted pressure transducers located in magnetic flow meters at upstream and downstream. The transducers are strain gauge type (Kyowa PGM-10KC) with the resonance frequency of 40kHz. The rotating speed of impeller is set at 1500rpm (f_n=25). The frequency is set 1,3 and 5Hz (f/f_n=0.04,0.12 and 0.20) at the mean flow rate ϕ=0.078.

3. Validation of Computational Results

Before carrying out unsteady calculations under the flow rate oscillation, several calculations were made with constant flow rates. Figure 5 shows the comparison of static pressure coefficient with experiments at various flow coefficients. The inlet (p_1) and outlet (p_2) static pressures are measured at z/D_t=-1.9 and z/D_t=0.55. Computational results show reasonable agreements with experiments. Figure 6 shows the comparison of the backflow length measured from the tip leading edge. The experimental results were obtained from cavitation tunnel experiments at σ=0.05 and N=3000rpm [1]. In LES results, the backflow length is evaluated from the location of the upstream edge of backflow region at r/R_t=0.96. These results show that present calculations predict the performance and the size of backflow reasonably.

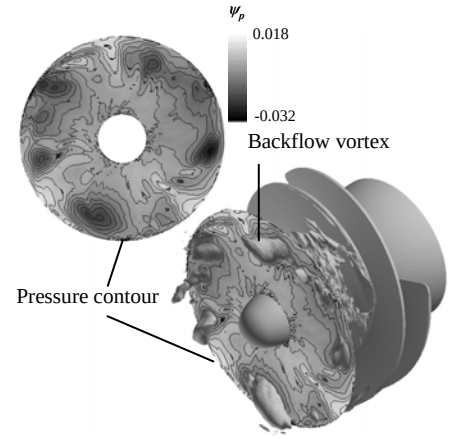

Fig. 7 Backflow vortex in LES

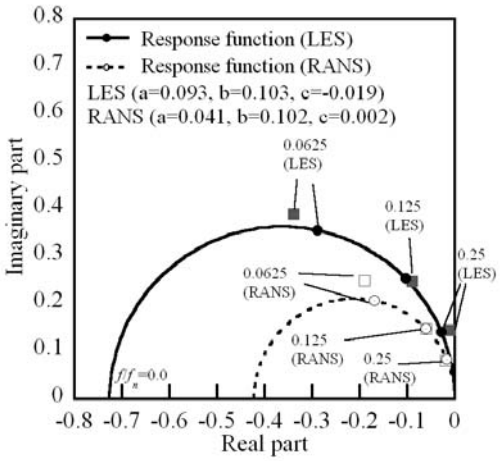

Fig. 8 Response function of backflow to flow rate fluctuation ($\tilde{A}/\tilde{\phi}$)

4. Response of the Backflow to the Flow Rate Oscillation

Yamamoto et al.[8,9] investigated the flow instabilities in a centrifugal cavitating pump and it was found that the phase delay of backflow vortex cavitation is closely related with cavitation surge. In order to investigate the relationship between the backflow vortex cavitation and cavitation surge, we need to understand the unsteady characteristics of backflow vortex cavitation. Thus, it is important to understand the response of backflow. In the present research, we investigated the response of backflow to the flow rate oscillation under the noncavitating condition.

We consider the flow rate oscillation

$$\phi=0.078+0.01\sin(2\cdot\pi\cdot f\cdot t) \quad (1)$$

where, the frequency of flow rate oscillation (f) is varied as 0.0625, 0.125 and 0.25 times the rotating frequency of inducer (f_n), considering the typical frequencies of cavitation surge (0.1~0.4 f_n). The amplitude of flow rate oscillation is about 13% of the design flow coefficient.

Qiao et al. studied the response of backflow to the flow rate fluctuation. However, they fail to simulate the backflow vortex structure because they used a turbulence model based on RANS. The present paper investigates the response of backflow to the flow rate oscillation under the existence of backflow vortex structure by using LES. Figure 7 shows backflow vortices visualized by the iso pressure surface corresponding to the vapor pressure at σ=0.04 and the pressure contour at z/D_t=-0.1.

Qiao et al. have shown that the size of the backflow region can be quantified by the angular momentum in a control volume set upstream of inducer. From the angular momentum conservation, they obtained the following response function.

$$\tilde{A}=-\frac{a+c}{b+j\cdot(2f/f_n)}\tilde{\phi} \quad (2)$$

where, $\tilde{A}$ is the complex amplitude of angular momentum in upstream, a is the proportional constant of the angular momentum supplied by the backflow and the flow rate oscillation, b is the proportional constant between the angular momentum removed by the normal flow and the angular momentum in upstream, c is the proportional constant between the angular momentum removed by the normal flow and the flow rate oscillation. Figure 8 compares the response functions with the values of parameters (a,b and c) determined from the LES and RANS calculations. The major difference between the results based on LES and RANS calculations is that the value of a from LES is twice as large as that from RANS. This means that the angular momentum supplied by backflow evaluated by LES is larger than that evaluated by RANS. The amplitude of angular momentum removal (b) by normal flow is nearly the same for both cases with negligible value of c. This results in the fact that the amplitude of angular momentum fluctuation based on LES is twice as larger as that based on RANS. Nearly the same value of b causes nearly the same phase delay of backflow. We should note that we do have a large phase delay even at the relatively low frequency of f/f_n=0.125. This large delay of backflow has been experimentally shown by Yamamoto [8] and has a effect to stabilize cavitation instabilities. Although we do have a large difference in the amplitude of angular momentum fluctuation, the quasi-steady axial length of the backflow region was nearly the same in LES and RANS simulation.

5. Unsteady Performance Curve

Several studies on unsteady flows in pumps have been reported. Ohashi [10] has investigated the dynamic response of the centrifugal pump, experimentally and theoretically. As a result, it was shown that the negative slope of the performance curve becomes smaller under unsteady condition. Kawata [11] has shown an example in which the negative gradient of performance curve under quasi-steady condition becomes positive under the unsteady condition, and causes surge. Lacopozzi et al.[12] have presented that the negative slope of performance curve in centrifugal pump becomes larger under the unsteady condition. Thus, the unsteady behavior of performance curve in a pump is not very clear. So, we focus on the unsteady performance.

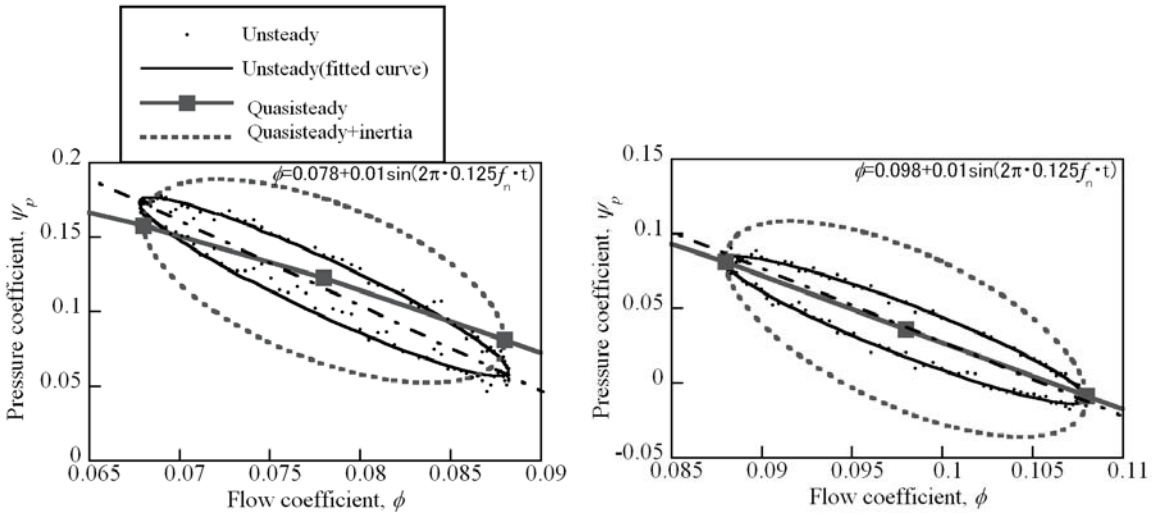

Fig. 9 Static pressure performance curve with flow rate fluctuation (Frequency of flow rate fluctuation; f=0.125 f_n,left; around design point, right; around higher flow rate)

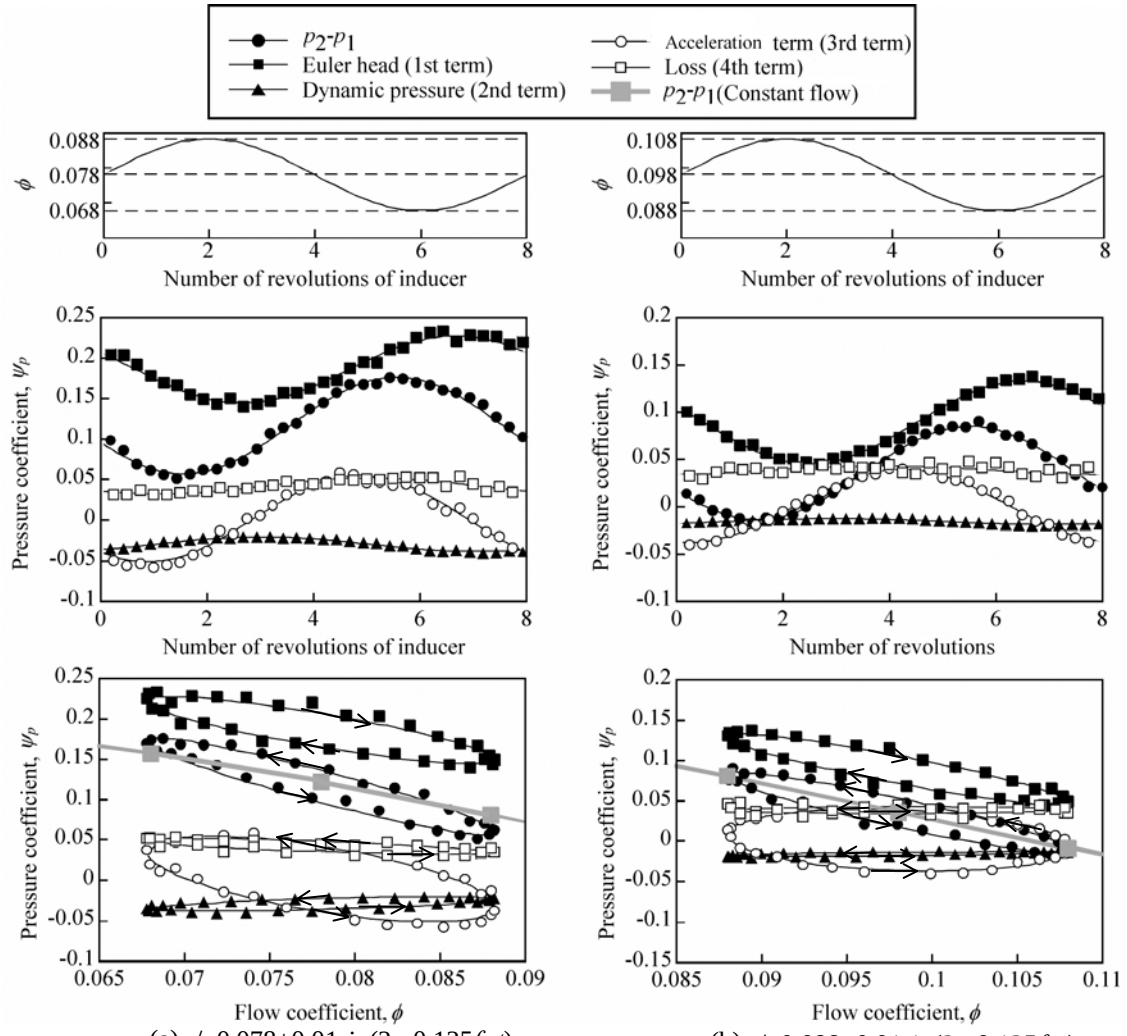

(a) ϕ=0.078+0.01sin(2π·0.125f_n·t) (b) ϕ=0.098+0.01sin(2π·0.125f_n·t)

Fig. 10 Each term of pressure equation (5)
(Top: Flow rate, center: temporal wave forms, Bottom Lissajous curves)

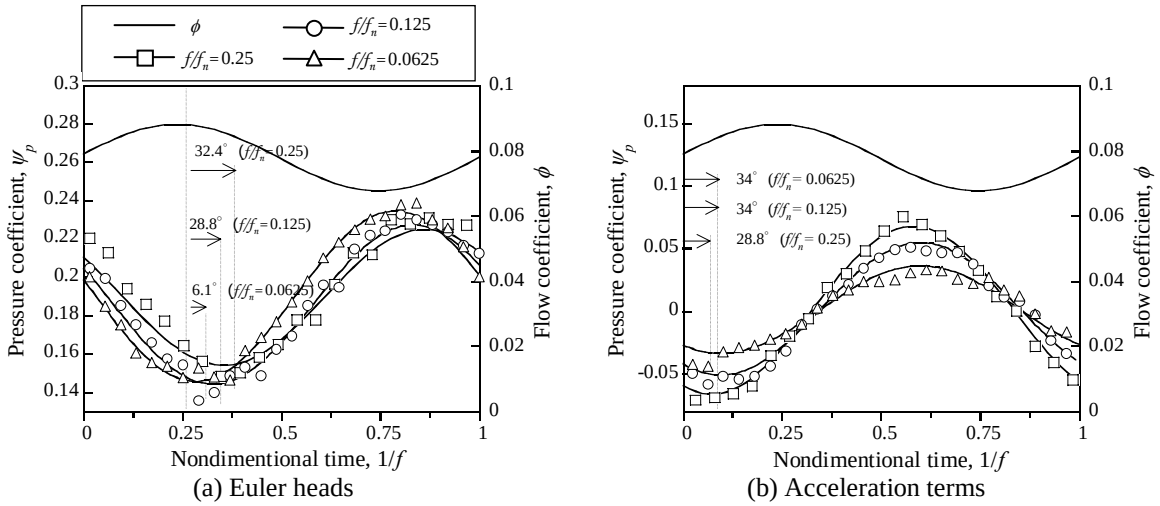

(a) Euler heads (b) Acceleration terms

Fig. 11 Effect of frequency on Euler's head and acceleration term, ϕ=0.078

Figure 9 shows the static pressure performance curve under the quasi-steady and unsteady conditions with the flow rate oscillations expressed as

ϕ=0.078 +0.01sin(2·π·0.125·t) ..... (3)

ϕ=0.098+0.01sin(2·π·0.125·t) ..... (4)

The dotted line shows the unsteady performance evaluated from the sum of quasi-steady performance and the pressure rise due to inertia. The pressure rise due to inertia is evaluated by assuming that axial velocity is uniform over each axial location and that the flow in the impeller is parallel to the blade. Firstly, we focus on the negative slope of unsteady performance curve. Around the design flow rate (ϕ=0.078), the negative slope of unsteady performance curve is larger than the quasi-steady result. This tendency is confirmed also for the f/f_n=0.25 and 0.0625 (not shown here). However, around higher flow rate (ϕ=0.098), the slope of performance curve is almost the same as the quasi-steady result. Secondly, we discuss about the width of Lissajous curve caused by the inertial effect. The inertia effect in LES is much smaller than that evaluated by the simplified method.

An equation for the evaluation of unsteady pressure rise was obtained by the following method. First, the unsteady torque on the impeller is determined from the unsteady angular momentum balance. Then, the unsteady work of impeller evaluated from the unsteady torque is equaled with the sum of the product of total pressure rise with the flow rate and the rate of the increase of kinetic energy in the control volume. The results obtained can be represented by

$$p_2 - p_1 = \frac{1}{Q}\left[\int_{out} \rho(r\omega)v_\theta v_z dA - \int_{in} \rho(r\omega)v_\theta v_z dA\right] - \frac{1}{2}\rho\left(v_2^2 - v_1^2\right) - \frac{1}{Q}\frac{d}{dt}\int \frac{1}{2}\rho w^2 dV - E_l \quad \text{..... (5)}$$

where, v is the absolute velocity, w is the relative velocity, the suffix numbers of 1 and 2 show the inlet and outlet. The first term on the right hand side corresponds to Euler's head, the second term represents the difference of dynamic pressure, the third term is associated with the increase of kinetic energy, and the last term is added to represent the effect of loss. The third term can be expressed as follows by using the cross-sectional area (dA) of the flow and the streamwise coordinate (ds):

$$-\frac{1}{Q}\frac{d}{dt}\int \frac{1}{2}\rho w^2 dV = -\frac{1}{Q}\int \rho w \frac{dw}{dt} dA ds = -\rho \int \left(\frac{wdA}{Q}\right)\frac{dw}{dt} ds \quad \text{..... (6)}$$

This expression shows that the term represents also the flow rate weighted average of the acceleration effect. So, we call it acceleration term. Equation (5) is very convenient for the discussion of the unsteady pressure rise. The fluctuation of each term in Eq.(5) are shown in Fig.10. The contributions of each term on the unsteady pressure performance are summarized as follows.

i) Euler's head: The Lissajous of Euler's head shows clockwise rotation caused by the delay in response. This shows that the Euler's head contributes to decrease the width of Lissajous curves of unsteady performance curve. The negative slope of Lissajous curve is smaller than the quasi-steady result. This suggests that the response delay of Euler's head reduces also the negative slope of performance curve. The delay of Euler's head is caused by free vortex shedding associated with the change of circulation [9]. The effect of frequency on Euler's head is shown in Fig.11(a). The delay is evident with a small decrease of amplitude.

ii) Change of dynamic pressure: The change of dynamic pressure is smaller than other terms.

iii) Acceleration: The acceleration term causes not only the width of the Lissajous but also the increase of negative slope. The negative slope of Lissajous curves at the design flow coefficient (ϕ=0.078) is larger than that at the higher flow rate (ϕ=0.098). The width of Lissajous curves for two mean flow rates (ϕ=0.078, ϕ=0.098) are almost the same and nearly equals the apparent pressure estimated by the simplified one dimensional inertial effect shown in Fig.9. The negative slope of Lissajous is caused by the delay of the acceleration term shown in Fig.11(b). The delay is found even at smaller frequency of f/f_n=0.0625 and is not significantly affected by the frequency. The amplitude increases with the frequency but the increase rate decreases at higher frequency.

iv) Loss: The loss term (E_l) is evaluated by subtracting the other terms in Eq.(5) from the pressure difference (p_2-p_1) actually obtained from the calculation. This term is nearly constant and does not contribute to the pressure rise oscillation.

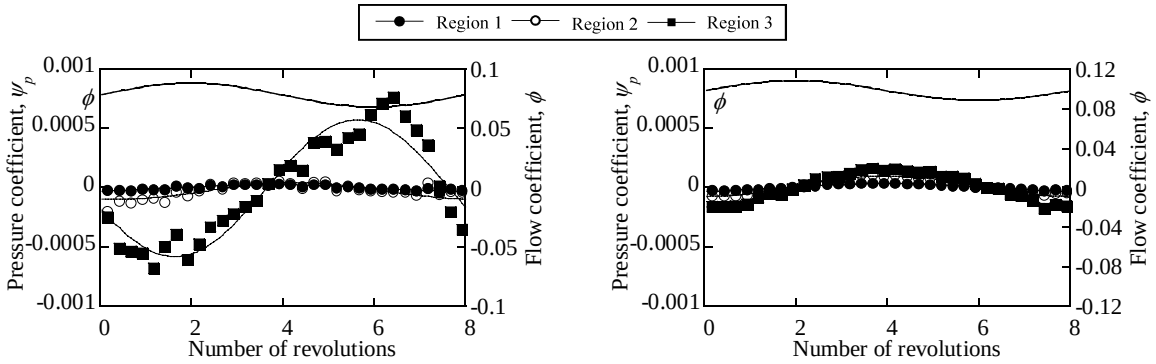

Fig. 12 Acceleration terms of equation (6) of upstream of inducer

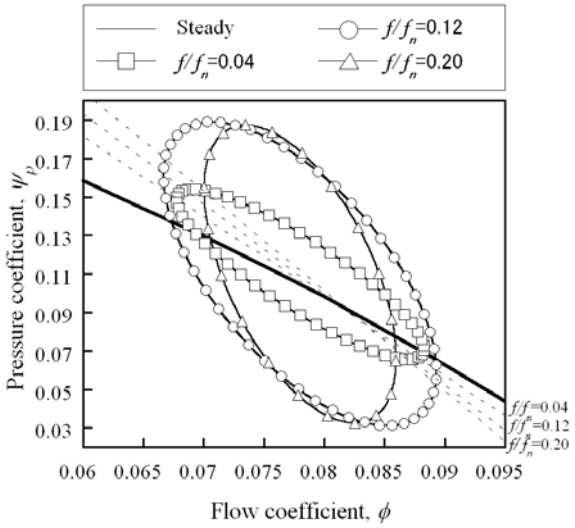

Fig. 13 Lissajous curves obtained by experiments

As mentioned above, it was found that the decrease of apparent inertial effect is caused by the response delay of Euler's head, and that the increase of negative slope of unsteady performance curve is caused by the delay of acceleration term. In order to investigate the cause of the delay of acceleration term, acceleration terms in the control volumes (Region 1, Region 2 and Region 3) shown in Fig.3 are calculated. The results are shown in Fig.12. Around the design flow rate (ϕ=0.078) in which the backflow appears (Fig.12(a)), the acceleration term in the Region 1 and Region 2 delays 90 degree behind the flow rate oscillation and is proportional to the acceleration. However, the response of acceleration term in Region 3 additionally delays 90 degree behind results of Region 1 and Region 2. Around higher flow rate (ϕ=0.098) where the backflow does not occur (Fig.12(b)), the acceleration term in all control volumes delays 90 degree behind the flow rate oscillation. Therefore, we can conclude that the delay of acceleration term is caused by the delay of backflow shown in Fig.8.

The experiments were made to validate the results. The experimental results are qualitatively compared with the computational results since the control volume includes not only the inducer but also the pipes between the two magnetic flow meters, as shown in Fig.4. The unsteady performance curves after curve fitting are shown in Fig.13. The negative slope of unsteady performance curve becomes larger as we increase the frequency. Even with the additional inertia of the piping system, the width of the Lissajous at f/f_n=0.12 is nearly the same as (Quasi-steady+inertia) in Fig.9. These results confirm that the negative slope increases and the inertia effects apparently decrease under flow rate fluctuations.

6. Conclusion

Investigations of the dynamic response of backflow and the unsteady performance curve by using LES under the noncavitating condition are carried out. The results are summarized as follows.

1) The amplitude of angular momentum supplied by the backflow was evaluated by LES to be twice as large as that evaluated by RANS. However, the phase delay of backflow is nearly the same.
2) At the design flow rate (ϕ=0.078) where the backflow appears, the negative slope of unsteady performance curve becomes larger with flow rate fluctuation than that at quasi-steady condition.
3) The pressure rise by the apparent inertial force obtained by LES is smaller than the simplified one dimensional estimation of inertial effect.
4) The decrease of the negative slope is caused by the delay of acceleration term due to the delay of backflow response, and the apparent decrease of inertia effect is caused by the delay of Euler's head.

5) At higher flow rate (ϕ=0.098) where the backflow dose not occur, only the decrease of apparent inertia effect due to the delay of Euler's head was observed.

Acknowledgement

The experiments were carried out with the help of Mr.Toshifumi Watanabe. The authors would like to thank his contributions. This study was made under the support of grant in aid for scientific research offered by JSPS.

Nomenclature

$\tilde{A}$	Complex magnitude of nondimensional angular momentum in upstream of inducer $= \int_V \rho r^2 v_\theta dr d\theta dz / (\rho U_t D_t^4)$	ρ	Density of water [kg/m^3]
		ϕ	Flow coefficient = v_z / U_t [-]
		σ	Cavitation number = $(p_1 - p_v) / (0.5\rho U_t^2)$ [-]
D_t	Diameter of inducer [m]	ψ_d	Pressure coefficient = $(p_2 - p_1) / (\rho U_t^2)$ [-]
f	Frequency of flow rate oscillation [Hz]		
f_n	Rotating frequency of inducer [Hz]		
p_1	Inlet pressure （ z= -1.9D_t） [Pa]		
p_2	Outlet pressure （ z= 0.55D_t） [Pa]		
r	Radial location [m]		
R_t	Radius of inducer [m]		
v_θ	Absolute circumferential velocity [m/sec]		
v_z	Absolute axial velocity [m/sec]		
U_t	Tip speed of the inducer [m/sec]		
z	Axial location [m]		

References

[1] Yokota, K., Kurahara, K., Kataoka, D., Tsujimoto, Y., 1998, "A study of Swirling Backflow and a Vortex Structure in the Inlet of an Inducer, " Journal of the Japan Society of Mechanical Engineers, 64-622, pp. 51-58.
[2] Qiao, X., Horiguchi, H., Tsujimoto, Y., 2007, "Response of Backflow to Flow Rate Fluctuations, ASME, Vol. 139, pp. 350-358.
[3] Yamanishi, N., Fukao, S., Qiao, X., Kato. C., Tsujimoto. Y., 2007, "LES simulation of Backflow vortex Structure at the Inlet of Inducer, ASME," Vol. 139, pp. 587-594.
[4] Acosta, A. J., 1958, "An Experimental Study of Cavitating Inducers," Proceedings of the Second Symposium on Naval Hydrodynamics, pp. 533-557.
[5] Acosta, A, Tsujimoto, Y., Yoshida, Y., Azuma, S., 2001, "Effects of Leading Edge Sweep on the Cavitation Characteristics of Inducer Pumps," International Journal of Rotating Machinery, Vol. 7, No. 6, pp. 397-404.
[6] Kamijo, K., Yoshida, M., Tsujimoto, Y.,1993, "Hydraulic and Mechanical Performance of LE-7 LOX Pump Inducer," Journal of Propulsion and Power, Vol. 9, No. 6.
[7] Kato, C., Kaiho, M., Manabe, A., 2003, "An Overset Finite-Element Large-Eddy Simulation Method with Applications to Turbomachinery and Aeroacoustics," ASME, Journal of Applied mechanics, Vol. 70, pp. 32-43.
[8] Yamamoto, K.,1992, "Instability in a Cavitating Centrifugal Pump_3rd Report: Mechanism of Low Cycle System Oscillation, " Journal of the Japan Society of Mechanical Engineers , 58-545, pp. 180-186.
[9] Yamamoto, K., Tsujimoto, Y., "A Backflow Vortex Cavitation and Its Effect on Cavitation Instabilities," International Journal of Fluid Machinery and Systems, Vol. 2, No. 1, pp. 40-54.
[10] Ohashi, H., 1968, "Analytical and Experimental study of Dynamic Characteristics of Turbopumps," NASA TN D-4298, pp. 1-109.
[11] Kawata, Y., Tanaka, T., Yasuda, O., Takeuchi, T., 1988, "Measurement of the transfer matrix of a prototype multi-stage centrifugal pump," ImechE, C346/88.
[12] Lacoppozi, M., Lingnarlol, V., Prevel, D.,1993, "Pogo Characterization of Ariane V Turbopump Lox Pump with Hot Water," AIAA-93-2134.